Calculations of the driving force of electromigration in hcp metals: Zn, Cd, Mg

Liang Lou, William L. Schaich, and James C. Swihart
Physics Department and Materials Research Institute, Indiana University, Bloomington, Indiana 47405
(Received 9 September 1985)

Using a pseudopotential, weak-scattering formalism we calculate the driving force for electromigration by the vacancy mechanism in the hcp metals Zn, Cd, and Mg. The general formula is evaluated in a succession of approximate models to illustrate the influence of different physical effects. The final results are compared both with the experimental data and with a previous evaluation for Zn. Our form factors, which have been fit to low-temperature data and then scaled to account for volume changes near the melting point, yield an effective valence for the wind force of about twice the experimental value and only in qualitative agreement with the observed anisotropy. Possible resolutions are discussed.

I. INTRODUCTION

The calculations presented here are motivated by the existence of experimental data for electromigration in the anisotropic metals Zn,[1,2] Cd,[3] and Mg.[4] For the first two cases the reported anisotropy in the driving force is greater than a factor of 2 in favor of motion in the basal plane, while for Mg the driving force is found to be nearly isotropic. Since, as we show below, the driving force can be viewed as an electronic transport property, it is interesting to examine whether the models that have been developed to explain anisotropic electrical resistivity in these systems can also account for the driving force anisotropies. We have specifically in mind the transport models developed by Swihart and co-workers,[5–8] which allow for anisotropies in both the energies and eigenstates of both the electrons and phonons in these crystals. The adaptation of these theories to the driving force of electromigration is formally straightforward within a pseudopotential, weak-scattering approach. Essentially the same ingredients are required, so comparison with the electromigration data is a useful further test of the theory.

A brief derivation of the necessary formulas is presented in Sec. II, based on the independent-particle, linear-response approach of Schaich.[9] There we describe in general terms the theoretical ingredients of the calculation and possible approximations for them. Detailed expressions are relegated to the Appendix. The formal theory, although different in approach, leads in the end to results similar to the theory presented by Genoni and Huntington[10] (GH), which was developed from earlier work of Huntington and co-workers.[2,11] The GH theory has only been applied to Zn and in order to obtain (nearly) analytic results, it introduces several simplifying approximations. Our theory is computationally more ambitious and does not need these approximations. Furthermore, we have added some refinements to and corrected some errors in GH's approach.

All of these various effects are illustrated numerically in Sec. III. By calculating the driving force in models of increasing sophistication, we show the qualitative influence of added effects and the quantitative uncertainty in our results. In general terms, the computed driving force is larger in magnitude and shows less anisotropy than the experimental data. Possible resolutions of these disagreements are discussed.

II. BASIC FORMULAS

There are many theoretical approaches to the driving force of electromigration; see the following reviews.[12–15] We feel that the linear-response formalism, first applied to this problem by Kumar and Sorbello,[16] offers the most powerful methods. In particular, it provides unambiguous and tractable ways to go beyond the study of an isolated impurity in jellium. This is important for our work since anisotropic effects require a detailed accounting of the discrete atomic structure washed out in jellium models.

In recent years, two distinct ways to include such effects have been evolving from the linear-response approach. The first is the one we use here.[2,9,10] It retains all scattering sites but assumes pseudopotentials and weak scattering. The second has a reversed emphasis.[17–21] It can treat arbitrarily strong scatterers within a muffin-tin-potential model but omits some of the possible scattering events[17,18] or sites.[19–21] This is most obvious in the finite-cluster models,[19–21] which retain only a small array of atoms around the moving atom of concern. Since Zn, Cd, and Mg can be reasonably treated as nearly free-electron systems, we shall not pursue the muffin-tin approach.

Starting with the Born-Oppenheimer approximation, we consider the force on an ion in the presence of an applied field when all the atoms are (momentarily) held stationary. Call $\mathbf{F}^D$ the part of the force that is linear in $\mathbf{E}$, the macroscopic, uniform, applied electric field. We separate $\mathbf{F}^D$ conceptually into two parts. The first part, $-Z_d e\mathbf{E}$, is called the direct force on the ion. Here $e<0$ is the electronic charge and Z_d is the ionic valence. For the systems of this paper, $Z_d=2$ since we assume that two electrons leave each atom to enter the conduction bands while the other electrons remain tightly bound in an ion core and simply act to screen out part $(Z-2)$ of the nuclear charge.[22]

The second part of $\mathbf{F}^D$ is due to the linear response of the conduction electrons. We call it the indirect (or wind) force and denote it by $\mathbf{F}_w^D$. Within an independent-electron model and in the weak-net-scattering limit,[9,23] it may be written as

$$\mathbf{F}_w^D = 2\sum_{\mathbf{k}} n_1(\mathbf{k}) \langle \psi_{\mathbf{k}}^+ | \mathbf{F} | \psi_{\mathbf{k}}^+ \rangle , \tag{1}$$

where $n_1(\mathbf{k})$ is the linear (in $\mathbf{E}$) disturbance in the distribution of electronic states and the matrix element is the expectation value of the force operator between an electron and the screened ion. One can write

$$\mathbf{F} = -\partial H/\partial \mathbf{R} , \tag{2}$$

where H is the adiabatic (ions fixed) Hamiltonian for the electrons and $\mathbf{R}$ locates the ion. The spin dependence of H is negligible,[5] so the only accounting for spin in (1) is the prefactor 2. The independent-particle states $|\psi_{\mathbf{k}}^+\rangle$ are scattered-wave states, formed from Bloch waves scattering off the defect complex surrounding an electromigrating ion. We assume the ion moves by a vacancy mechanism; so in midjump the defect complex has a displaced ion plus lattice vacancies at both ends of its jump path and possibly further distortions in other atoms' locations. We consider only an isolated defect and denote its modification of the crystal's potential energy by U; therefore

$$H = H_0 + U , \tag{3}$$

where H_0 is the perfect-crystal Hamiltonian, whose eigenstates are the Bloch waves $|\phi_{\mathbf{k}}\rangle$ of energy $\epsilon_{\mathbf{k}}$.

A key feature of our approach is that each electron-ion interaction energy is represented by a pseudopotential. We assume that every atom rigidly carries the same, spherically symmetric, screened interaction energy w centered on its nuclear position. Thus, H and U are completely specified once w and all the ion locations are given. We remark that GH formally allowed the w's to vary among ions and to lack spherical symmetry, due to differences in screening. However, in their calculations this generalization is suppressed. It is not clear how large an effect is thereby being omitted. In muffin-tin models[17–21] even more drastic approximations to the form of the interaction energy are necessary. Another technical point worth noting is that the use of pseudopotentials and pseudo-wave-functions to evaluate (1) can formally yield the exact result, at least within the orthogonalized-plane-wave (OPW) formalism.[24,25] However, the nonlocal semiempirical pseudopotentials with which we calculate are not strictly derived from OPW theory; so their application in (1) as well as for the electron-phonon interaction is an approximation.

Outweighing the above uncertainties is the advantage that with pseudopotentials we can determine the $|\psi_{\mathbf{k}}^+\rangle$ by perturbation theory:

$$|\psi_{\mathbf{k}}^+\rangle = |\phi_{\mathbf{k}}\rangle + \sum_{\mathbf{k}'} |\phi_{\mathbf{k}'}\rangle \frac{\langle \phi_{\mathbf{k}'} | U | \phi_{\mathbf{k}} \rangle}{\epsilon_{\mathbf{k}} - \epsilon_{\mathbf{k}'} + i0^+} + \cdots . \tag{4}$$

Combining this expansion with the symmetries

$$n_1(\mathbf{k}) = -n_1(-\mathbf{k}) , \tag{5}$$

$$\epsilon_{\mathbf{k}} = \epsilon_{-\mathbf{k}} , \tag{6a}$$

$$\langle \phi_{\mathbf{k}} | O | \phi_{\mathbf{k}'} \rangle = \langle \phi_{-\mathbf{k}'} | O | \phi_{-\mathbf{k}} \rangle = \langle \phi_{\mathbf{k}'} | O | \phi_{\mathbf{k}} \rangle^* , \tag{6b}$$

where O is either U or $\mathbf{F}$, we can rewrite (1) as

$$\mathbf{F}_w^D = -4\pi \sum_{\mathbf{k},\mathbf{k}'} n_1(\mathbf{k}) \delta(\epsilon_{\mathbf{k}} - \epsilon_{\mathbf{k}'}) \times \mathrm{Im}(\langle \phi_{\mathbf{k}} | U | \phi_{\mathbf{k}'} \rangle \langle \phi_{\mathbf{k}'} | \mathbf{F} | \phi_{\mathbf{k}} \rangle) . \tag{7}$$

Here Im denotes "imaginary part of" and $\mathbf{F}_w^D$ is clearly real.

We assume n_1 is determined by a constant-relaxation-time approximation

$$n_1(\mathbf{k}) = \sum_{\alpha} e\mathbf{E}^{\alpha} \cdot \left(-\frac{\partial n_0}{\partial \hbar \mathbf{k}} \right) \tau^{\alpha} , \tag{8}$$

where $\hbar$ is Planck's constant over 2π and $n_0(\mathbf{k})$ is the electron-distribution function in equilibrium. We have written (8) in a form appropriate to an hcp symmetry: $\mathbf{E}^{\alpha}$ is the part of $\mathbf{E}$ along (or orthogonal to) the c axis for α equal to $\parallel$ (or $\perp$). Studies of the resistivity[5–7] show that this form of n_1 is reasonable at the high temperatures of the electromigration experiments. On the other hand the temperature broadening of $\partial n_0/\partial \mathbf{k}$ is still negligible so we use

$$-\frac{\partial n_0}{\partial \hbar \mathbf{k}} = \mathbf{v}_{\mathbf{k}} \delta(\epsilon_{\mathbf{k}} - \epsilon_F) , \tag{9}$$

where ϵ_F is the Fermi energy and $\mathbf{v}_{\mathbf{k}}$ is the group velocity of Bloch state $\mathbf{k}$. Incorporating (8) and (9) into (7) yields

$$\mathbf{F}_w^D = -4\pi \sum_{\alpha} e\tau^{\alpha} \sum_{\mathbf{k}} \delta(\epsilon_{\mathbf{k}} - \epsilon_F) \sum_{\mathbf{k}'} \delta(\epsilon_{\mathbf{k}'} - \epsilon_F) \mathrm{Im}(\langle \phi_{\mathbf{k}} | U | \phi_{\mathbf{k}'} \rangle \langle \phi_{\mathbf{k}'} | \mathbf{F} | \phi_{\mathbf{k}} \rangle) \mathbf{v}_{\mathbf{k}} \cdot \mathbf{E}^{\alpha} = \vec{f}(\mathbf{R}) \cdot \mathbf{E} , \tag{10}$$

which gives the indirect driving force on a migrating ion at $\mathbf{R}$ in terms of a pair of integrals over the Fermi surface. Equation (10) defines $\vec{f}(\mathbf{R})$.

The τ^{α} in (10) are determined by fitting to the experimental resistivities. Using (8) and (9) the induced-current density is

$$\begin{aligned} \mathbf{J} &= \frac{2}{\Omega} \sum_{\mathbf{k}} e\mathbf{v}_{\mathbf{k}} n_1(\mathbf{k}) \\ &= \frac{2e^2}{\Omega} \sum_{\mathbf{k}} \delta(\epsilon_{\mathbf{k}} - \epsilon_F) \mathbf{v}_{\mathbf{k}} \sum_{\alpha} \tau^{\alpha} \mathbf{v}_{\mathbf{k}} \cdot \mathbf{E}^{\alpha} \\ &= \frac{ne^2}{m} \sum_{\alpha} \tau^{\alpha} X^{\alpha} \mathbf{E}^{\alpha} = \sum_{\alpha} \sigma_{\alpha\alpha} \mathbf{E}^{\alpha} , \end{aligned} \tag{11}$$

where Ω is the system volume, n the average conduction-electron density, m the free-electron mass, and $\sigma_{\alpha\alpha}$ a conductivity component. We calculate the X^α defined implicitly above as a single integral over the Fermi surface. Then we use them and the measured $\sigma_{\alpha\alpha}$ and n to fix the τ^α.

In an isotropic jellium model, $\overleftrightarrow{f}(\mathbf{R})$ in (10) is a diagonal tensor characterized by a single, $\mathbf{R}$-independent number, Z_w:

$$\overleftrightarrow{f}(\mathbf{R}) = -Z_w e \overleftrightarrow{1} . \tag{12}$$

Our general result (10) is clearly more complex. Since both U and $\mathbf{F}$ depend on $\mathbf{R}$ we have not been able to prove that $\mathbf{F}_w^D(\mathbf{R})$ is a conservative force unless only single plane waves are used for the Bloch pseudo-wavefunctions.[25] Indeed our calculations show that the work done by $\mathbf{F}_w^D(\mathbf{R})$ is path dependent. However, as discussed further in the Appendix, the quantitative variations are not significant so we will be able to apply the usual theory of driven diffusion[26] in Sec. III. Toward this end we now assume that

$$\int_{\mathbf{R}_1}^{\mathbf{R}_2} d\mathbf{R}' \cdot \mathbf{F}_w^D(\mathbf{R}') = -\sum_\alpha Z_w^{\gamma,\alpha} e \mathbf{E}^\alpha \cdot (\mathbf{R}_2 - \mathbf{R}_1) ; \tag{13}$$

i.e., that the work done by the indirect induced force on an ion as it moves (in a straight line) from one lattice site $\mathbf{R}_1$ to another $\mathbf{R}_2$ is the same as if it were in a constant force field $-\sum_\alpha Z_w^{\gamma,\alpha} e \mathbf{E}^\alpha$. Here the wind contribution to the effective valence $Z_w^{\gamma,\alpha}$ depends on both the orientation of $\mathbf{E}$, as described by α, and the type of jump, as described by γ. For motion by the vacancy mechanism in hcp crystals, there are two possible values of γ. In each case the atom jumps to a nearest neighbor site. For $\gamma = B$ the jump lies within the basal plane while for $\gamma = A$ it goes to one of the planes adjacent to the basal plane. Thus we have three values of effective valence: $Z_w^{B,\perp}$, $Z_w^{A,\parallel}$, and $Z_w^{A,\perp}$.[27] The need for an independent $Z_w^{A,\perp}$ is ignored by GH, although only for an isotropic system does $Z_w^{A,\perp}$ equal $Z_w^{A,\parallel}$. The complication of (13) compared to (12) has not been acknowledged before, and in Sec. III we show how to relate these anisotropy parameters to the experimental anisotropies in driving forces, diffusion constants, and resistivities. Here we emphasize that (13) is a simplification of the content of (10).

In general terms the computational task is now clear. We expand the Bloch pseudo-wave-functions in a plane-wave expansion

$$|\phi_{\mathbf{k}}\rangle = \sum_{\mathbf{G}} a_{\mathbf{G}}(\mathbf{k}) |\mathbf{k}+\mathbf{G}\rangle , \tag{14}$$

where the $\mathbf{G}$ are reciprocal-lattice vectors. The number of terms in this expansion that one retains in the calculation either of $\epsilon_{\mathbf{k}}$, $\mathbf{v}_{\mathbf{k}}$, and the Fermi surface, or of the matrix elements of (10) determine the magnitude of the task and the accuracy, at least within the model, of the results.

Before describing these we wish to comment on further influences of temperature. In order to enhance the ionic mobility, electromigration measurements are done close to the melting temperature. We account for this elevated temperature in the calculation of the band structure in several ways. The most obvious is to use the high-temperature lattice constants. A second modification is less straightforward and involves a rescaling of the screened pseudopotential form factors, which have been fit to low-temperature data, in order to account for the reduced electron density at high temperature. The detailed procedure is described later. These first two modifications produce only small corrections and are of no qualitative importance.

A third modification is potentially more interesting. It involves using the Debye-Waller factor (DWF) to reduce pseudopotential form factors. In a nearly free-electron system, the inclusion of such factors is the dominant modification[28] of the band structure, and we include it as do GH. One might be tempted to go further to multiply the matrix elements of U and $\mathbf{F}$ in (10) by DWF's. This extension makes a non-negligible contribution to the anisotropy since, e.g., in Zn the mean-square vibration amplitude is a factor of 3 greater along the c axis than in the basal plane.[29] However we feel that no DWF should multiply the form factor associated with the ion on which one is computing the force. Our reasoning is based on the Born-Oppenheimer approximation, which requires one to hold all the ions stationary while finding the electronic states. Within this viewpoint the inclusion of a DWF with any ion accounts for the (static) uncertainty in its location. Averaging the $\mathbf{F}_w^D$ of (10) over the uncertainty of the surrounding ions is correct, but an average over the location of $\mathbf{R}$ should be accounted for only by the integral (13). The numerical consequences of these remarks are illustrated in Table V.

III. RESULTS AND DISCUSSION

We begin by showing in Fig. 1 the form factors, $w(\mathbf{k}',\mathbf{k})$, used in the calculations. Since the pseudopotentials we employ are nonlocal, one must specify more than

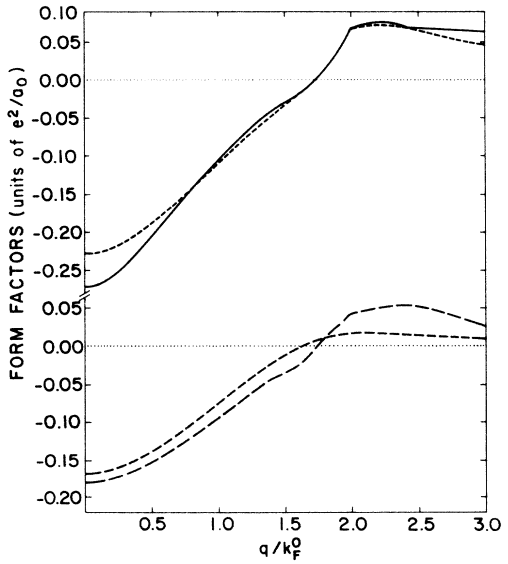

FIG. 1. Pseudopotential form factor w versus wave-vector transfer $\mathbf{q}$. The lengths of $\mathbf{k}$ and $\mathbf{k}'$ are specified in the text. The w have been scaled to the temperatures of Table I and are labeled as in the Appendix: Zn (SOMP), ——; Zn (AWSF), ----; Cd (AWSF), — —; Mg (AWSF), — — —.

TABLE I. Basic parameters. a_0 is the Bohr radius.

Metal	T range[a] (K)	T (K)	a (Å)	c (Å)	k_F^0 (Units of $1/a_0$)	ϵ_F^0 (Units of e^2/a_0)	$\langle u_a^2 \rangle$ (Units of a_0^2)	$\langle u_c^2 \rangle$ (Units of a_0^2)
Zn	639–673	650	2.67[b]	5.05	0.826	0.341	0.046[d]	0.137
Cd	488–563	530	3.00[c]	5.71	0.733	0.269	0.043[e]	0.137
Mg	773–853	810	3.25[c]	5.28	0.714	0.255	0.101[f]	0.104

[a]Reference 12.
[b]Reference 30.
[c]Reference 31.
[d]Reference 29.
[e]Reference 32.
[f]Reference 33.

the wave-vector change, $\mathbf{q}=\mathbf{k}'-\mathbf{k}$, when describing $w(\mathbf{k}',\mathbf{k})$. In Fig. 1 we set $|\mathbf{k}'|=|\mathbf{k}|=k_F^0$ for $|\mathbf{q}|<2k_F^0$, where k_F^0 is the free-electron Fermi wave vector. This arrangement dominates the calculation of the Z's. For $|\mathbf{q}|>2k_F^0$, we use in Fig. 1 a backscattering configuration in which $\mathbf{k}$ and $\mathbf{k}'$ are antiparallel and $|\mathbf{k}|=k_F^0$ while $|\mathbf{k}'|=|\mathbf{q}|-k_F^0$. This change of presentation at $|\mathbf{q}|=2k_F^0$ is responsible for the discontinuous slope in w in Fig. 1. For Zn we calculate for two different choices of w. As described in the Appendix, these differ only away from the important nonzero reciprocal-lattice vectors. Hence they produce the same band structure, to within a constant energy shift, but different Z_w's. All the w's have been determined at a temperature in the middle of the range spanned by the electromigration experiments. These temperature values are summarized in Table I along with the lattice constants and free-electron parameters k_F^0 and ϵ_F^0.

The form factors are derived from fits to low-temperature data, which are then scaled to near the melting point. To give some sense of their high-temperature accuracy, we used them to calculate the resistivity of the liquid metals. We employed the Ziman formula[34,35] and our form factors scaled to just above the melting point. They differ from those shown in Fig. 1 by less than a couple percent. The liquid-structure factor was approximated by the hard-core Percus-Yevick solution with packing fraction $\eta=0.456$.[36] Our results are collected in Table II and suggest that w is somewhat too strong in Zn and Cd but too weak in Mg. Small changes in the w's near $q\sim 2k_F^0$ could remove the discrepancies, but we shall not attempt such (nonunique) tampering. Instead we stress that the Z_w's, like the liquid-metal resistivities, depend sensitively on the strength of the backscattering form factor.

In calculating the high-temperature band structures, two local (only $|\mathbf{q}|$ dependent) factors multiply the w's in the secular determinant [see Eq. (A2)]. The first, described in the Appendix, is the unit-cell structure factor and the second is a DWF. The latter is defined for hcp systems by

$$D(\mathbf{q})=\exp[-\tfrac{1}{2}\langle u_c^2\rangle q_z^2-\tfrac{1}{2}\langle u_a^2\rangle(q_x^2+q_y^2)]\ , \qquad (15)$$

where the z direction is along the c axis. The mean-square vibration amplitudes that we use are listed in Table I. For large $|\mathbf{q}|$, the DWF reduces the form factor by over 20% and does so anisotropicly.

We have now assembled the ingredients for the major microscopic calculations of this paper. To clarify the dependence of the $Z_w^{\gamma,\alpha}$ of (13) we separate them as

$$Z_w^{\gamma,\alpha}=A^{\gamma,\alpha}/\rho_{\alpha\alpha}X^{\alpha}\ , \qquad (16)$$

where the X^{α} are defined in (11) and (A5) and $\rho_{\alpha\alpha}=1/\sigma_{\alpha\alpha}$ are resistivity components. The X^{α} are determined by the band structure alone, while the $A^{\gamma,\alpha}$, more explicitly defined in the Appendix, depend on the scattering from the defect complex created by the electromigrating ion. Both the X^{α} and $A^{\gamma,\alpha}$ are calculated by numerical Monte Carlo integrations.[5–8] Since the X^{α} require only one such integral over the Fermi surface while the $A^{\gamma,\alpha}$ require double integrals, the former are essentially exact (through three digits) while the latter are determined to within $\pm 4\%$, which is sufficient given the uncertainty in the pseudopotentials.

The results are collected in Tables III(a)–III(c) for up to seven different cases. These vary in sophistication of treatment. In the first four cases a single plane wave (PW) is used for each Bloch pseudo-wave-function that appears in the matrix elements, while in the next two cases a sum of two plane waves is used and in the last case three plane waves. The resulting $A^{\gamma,\alpha}$ appear to have converged satisfactorily. The a_G's used in these expansions of the matrix elements are the largest ones from the band-structure expansions, which are then scaled to insure normalized $|\phi_{\mathbf{k}}\rangle$. In calculating the band structure we use up to eight terms in the expansion (14). These best calculations appear in cases 4, 6, and 7. At the other extreme, case 1 represents the free-electron limit. For cases 3 and 5 a two-plane-wave expansion is used to generate the Fermi surface. The nonzero reciprocal-lattice vectors are either (002) or (101), depending on which Bragg plane has the greater influence.[10,11] Finally, in case 2 we re-

TABLE II. Resistivity of liquid metal (Ref. 37).

Metal	T_{melt} (K)	ρ_{expt} ($\mu\Omega$ cm)	ρ_{theor} ($\mu\Omega$ cm)
Zn (SOMP)	693	37.4	47.9
Zn (AWSF)	693	37.4	49.3
Cd (AWSF)	594	33.7	51.5
Mg (AWSF)	923	27.4	16.4

TABLE III. Results of microscopic calculations for (a) Zn (SOMP, AWSF), (b) Cd (AWSF), and (c) Mg (AWSF). The pair of numbers in the A columns correspond to using the SOMP and AWSF pseudopotentials, respectively.

Case	Fermi surface	ϵ_F (units of e^2/a_0)	Matrix elements	$X^{\|\|}$	$X^{\perp}$	$-A^{A,\|\|}$ ($\mu\Omega$ cm)	$-A^{A,\perp}$ ($\mu\Omega$ cm)	$-A^{B,\perp}$ ($\mu\Omega$ cm)
			(a) Zn (SOMP, AWSF)					
1	Perfect sphere	0.341	1 PW	1	1	149,165	149,165	134,150
2	Truncated sphere	0.341	1 PW	0.676	0.459	48,53	36,41	36,40
3	2 PW's	0.390	1 PW	0.623	0.461	62,68	47,53	49,55
4	Many PW's	0.387	1 PW	0.605	0.399	66,72	47,53	49,54
5	2 PW's	0.390	2 PW	0.623	0.461	61,66	48,53	44,48
6	Many PW's	0.387	2 PW	0.605	0.399	62,67	47,52	42,47
7	Many PW's	0.387	3 PW	0.605	0.399	−,66	−,53	−,46
			(b) Cd (AWSF)					
1	Perfect sphere	0.269	1 PW	1	1	211	211	191
2	Truncated sphere	0.269	1 PW	0.663	0.471	53	41	40
3	2 PW's	0.316	1 PW	0.591	0.489	83	72	72
4	Many PW's	0.313	1 PW	0.551	0.427	86	72	75
5	2 PW's	0.316	2 PW	0.591	0.489	73	63	62
6	Many PW's	0.313	2 PW	0.551	0.427	72	66	65
7	Many PW's	0.313	3 PW	0.551	0.427	71	65	62
			(c) Mg (AWSF)					
1	Perfect sphere	0.255	1 PW	1	1	106	106	106
2	Truncated sphere	0.255	1 PW	0.782	0.713	56	56	56
3	2 PW's	0.231	1 PW	0.652	0.686	77	78	79
4	Many PW's	0.230	1 PW	0.657	0.586	78	76	76
5	2 PW's	0.231	2 PW	0.652	0.686	68	72	66
6	Many PW's	0.230	2 PW	0.657	0.586	69	69	63
7	Many PW's	0.230	3 PW	0.657	0.586	70	69	60

move the portions of the free-electron Fermi sphere in the directions that have no Fermi surface in case 4. In the directions where the Fermi surface remains, both the Fermi wave vector and velocity are given their free-electron values.

Thus between case 1 and 2 we account for the missing solid angles in the true Fermi surface, without including distortions. This effect significantly reduces both the X^{α} and $A^{\gamma,\alpha}$ and is the dominant source of the anisotropies. Going from case 2 to either case 3 or 4 slightly decreases the X^{α} and increases the $A^{\gamma,\alpha}$. We view this as a consequence of reductions in the velocity over the remaining, now distorted, Fermi surface. From (A5) one has that $X^{\alpha} \propto v$, while (A8) implies that $A^{\gamma,\alpha} \propto 1/v$, where v is a typical Fermi-surface velocity. Improving the treatment of the matrix elements in cases 5–7 only slightly reduces the $A^{\gamma,\alpha}$. Similarly the changes between cases 3 and 4 (or between cases 5 and 6), are not large. Hence a reasonable estimate of both the X^{α} and $A^{\gamma,\alpha}$ can be made already at the case-3 level: a two-plane-wave treatment of the Fermi surface and single plane waves in the matrix elements. In GH, analogues of cases 2, 3, and 5 for Zn alone were treated.

From Table III (a) we see that the two form factors for Zn yield the same Fermi surface and X^{α}, but $A^{\gamma,\alpha}$ that differ by about 10%. Comparing between tables, the results indicate slightly stronger scattering in Cd than Zn. This is not obvious from Fig. 1, until one notes that the Fermi energy in Cd is significantly smaller than that in Zn and that the ratio of w/ϵ_F is a better measure of scattering strength. Figure 1 does show that in Mg the scattering is weaker than in either Zn or Cd and as a consequence the anisotropies in X^{α} and $A^{\gamma,\alpha}$ in Table III (c) are less. The X^{α} for Mg are larger for cases 2–7 because there is no longer a large hole in the Fermi surface around the ΓL direction.[5,7] This extra Fermi-surface area also counters the reduced scattering strength so that the $A^{\gamma,\alpha}$ in Mg have roughly the same magnitude as those in Cd.

Turning now to a comparison with experiment, we must do more than the simple calculation of (16). The necessary analysis requires some diffusion theory,[26,38,39] of which we only present the key formulas.[3] The correlated motion of atoms by the vacancy mechanism in hcp systems is described by the diffusion constants

$$D_{\|}^{*} = \tfrac{3}{4} p c^2 \Gamma_A f_A \ , \tag{17}$$

$$D_{\perp}^{*} = \tfrac{3}{2} p a^2 \Gamma_B f_B + \tfrac{1}{2} p a^2 \Gamma_A f_A \ , \tag{18}$$

where p is the probability that an atom has a vacancy in a nearest-neighbor site, Γ_{γ} are jump frequencies for the two possible kinds of jumps, and f_{γ} are correlation factors. In an applied field the directed motion is not correlated and is described by

TABLE IV. Comparison of experiment and theory.

Metal	a^2/c^2	$D_{\parallel}^*/D_{\perp}^*$	f_A[d]	f_B[d]	$\rho_{\parallel}$[e] ($\mu\Omega$ cm)	$\rho_{\perp}$[e] ($\mu\Omega$ cm)	$-\left(\frac{Z^*}{f}\right)_{\parallel}^{\text{expt}}$	$-\left(\frac{Z^*}{f}\right)_{\perp}^{\text{expt}}$	$-\left(\frac{Z^*}{f}\right)_{\parallel}^{\text{theor}}$	$-\left(\frac{Z^*}{f}\right)_{\perp}^{\text{theor}}$
Zn (AWSF)	0.280	1.69[a]	0.77	0.79	15.2	14.5	2.55±0.15[f]	5.6±0.4	6.8	8.0
Cd (AWSF)	0.277	1.63[b]	0.78	0.79	16.8	14.1	2.0±0.2[g]	4.1±0.4	7.3	10.8
Mg (AWSF)	0.379	0.81[c]	0.81	0.75	13.2	15.9	2.03±0.2[h]	2.03±0.2	7.4	6.1

[a]Reference 40.
[b]Reference 41.
[c]Reference 42.
[d]Reference 39.
[e]Reference 43.
[f]Reference 1.
[g]Reference 3.
[h]Reference 4.

$$D_{\parallel}^*\left(\frac{Z^*}{f}\right)_{\parallel}=\tfrac{3}{4}pc^2\Gamma_A Z^{A,\parallel}\,, \tag{19}$$

$$D_{\perp}^*\left(\frac{Z^*}{f}\right)_{\perp}=\tfrac{3}{2}pa^2\Gamma_B Z^{B,\perp}+\tfrac{1}{2}pa^2\Gamma_A Z^{A,\perp}\,. \tag{20}$$

Here the D_α^* are those in (17) and (18) while the $(Z^*/f)_\alpha$ are new parameters. Only the ratios $(Z^*/f)_\alpha$ are determined experimentally.[12] The $Z^{\gamma,\alpha}$ are what one can calculate from (16) as

$$Z^{\gamma,\alpha}=Z_w^{\gamma,\alpha}+Z_d\,. \tag{21}$$

Eliminating the $p\Gamma_\gamma$ from (17)—(20) yields

$$\left(\frac{Z^*}{f}\right)_{\parallel}=Z^{A,\parallel}/f_A\,, \tag{22}$$

$$\left(\frac{Z^*}{f}\right)_{\perp}=Z^{B,\perp}/f_B-\frac{2}{3}\frac{a^2}{c^2}\frac{D_{\parallel}^*}{D_{\perp}^*}(Z^{B,\perp}/f_B-Z^{A,\perp}/f_A)$$

$$=Z^{B,\perp}/f_B-\Delta\,. \tag{23}$$

The contribution of Δ is omitted by GH. We find that $0<\Delta\leq 0.5$.

In Table IV we collect the numbers needed to evaluate (21)—(23). The D_α^* and $\rho_{\alpha\alpha}$, as well as a^2/c^2 from Table I, are taken from experimental data, while the f_γ are from Mullen's calculation.[39] We also list the measured values of $(Z^*/f)_\alpha$ along with their uncertainties. The calculated $(Z^*/f)_\alpha$ are each based on case 7 from the appropriate Table III. All the calculated $(Z^*/f)_\alpha$ appear too large in magnitude. Using the SOMP form factor of Zn makes only a slight improvement. With respect to anisotropy, Mg is certainly different from Zn and Cd but for none of the metals does the amount of anisotropy match well with experiment.

As mentioned in Sec. II, one possible way to reduce these disagreements is via the Debye-Waller factor. This is illustrated in Table V, which shows the effect of the DWF on case-3 calculations for Zn (AWSF)—see Table III(a). We list the calculated $Z_w^{\gamma,\alpha}$ for possible forms of the matrix elements. The general definition of **B** appears in the Appendix, and in Table V we modify its single plane-wave form (A16). In the first row no DWF appears; in the second the correct formula is used; and in the third every form factor is multiplied by a DWF. The third prescription yields significantly smaller and more anisotropic $Z_w^{\gamma,\alpha}$. However, as argued before, the proper calculation appears in the second line. The slight difference between the numbers in the second and first row suggests that a better theory of thermal effects in the matrix elements, such as is used in extended x-ray absorption fine structure[44,45] is not warranted here. For comparison, we also list in the fourth row of Table V the results quoted by GH for the same $Z_w^{\gamma,\alpha}$, with the caution that they used a different interpolation to obtain their form factor and different values of τ^α taken from earlier calculations[11] rather than fit to experiment. Although their paper does not explicitly state how DWF's were included, T. C. Genoni has informed us (private communication) that the prescription

TABLE V. Effect of Debye-Waller factor.

B form	$-A^{A,\parallel}$ ($\mu\Omega$ cm)	$-A^{B,\perp}$ ($\mu\Omega$ cm)	$-Z_w^{A,\parallel}$	$-Z_w^{B,\perp}$
$-qw^2\left[1-2\frac{\sin(\mathbf{q}\cdot\mathbf{R}^\gamma)}{\mathbf{q}\cdot\mathbf{R}^\gamma}\right]$	68	54	7.2	8.0
$-qw^2\left[1-2D\frac{\sin(\mathbf{q}\cdot\mathbf{R}^\gamma)}{\mathbf{q}\cdot\mathbf{R}^\gamma}\right]$	68	55	7.2	8.2
$-qw^2D^2\left[1-2\frac{\sin(\mathbf{q}\cdot\mathbf{R}^\gamma)}{\mathbf{q}\cdot\mathbf{R}^\gamma}\right]$	51	45	5.4	6.8
GH	49	39	5.0	6.7

of the first row was used. Still the $Z_w^{\gamma,\alpha}$ in the fourth row agree better with those in the third row than with those in either the first or second row. We can not explain this anomaly.

Returning to the comparison with experiment, it is not clear where to find a resolution; i.e., whether the dominant error lies in experiment, or in the formal or practical theory. By "practical theory" we mean the task of calculating our basic formula, (10). One can significantly "improve" the answers for the $Z_w^{\gamma,\alpha}$ by modifying the most crucial ingredients, the form factors; but this would be unsatisfactory since the empirical pseudopotentials we use have already been fit to other data. A second alternative is that our basic formula is wrong. The key assumption in its derivation is that a perturbative treatment of an undistorted defect complex is valid. To either prove or disprove this ansatz is a difficult task. One could study the effect of lattice distortions without much extra effort, but to go beyond perturbation theory in a systematic, quantitative way is beyond present theoretical capabilities. Finally we raise the possibility that the experiments may be in error. For each metal the measurements were only done once and all by the same technique. The data for Mg are the most suspect to us, since the experimental description notes special difficulties. Renewed experimental study should focus first on Mg.

ACKNOWLEDGMENTS

We wish to thank Professor H. B. Huntington and Professor T. C. Genoni for helpful discussions. This work was supported in part by NSF under Grant No. DMR 81-15705 and No. DMR 81-17013. One of us (J.C.S.) wishes to thank the Metals and Ceramics Division of Oak Ridge National Laboratory for its hospitality while part of this work was carried out as sponsored by the Division of Materials Sciences, U.S. Department of Energy under Contract No. De-AC05-840R21400 with the Martin Marietta Energy Systems, Inc.

APPENDIX

Here we develop more explicit expressions from the general formulas of Sec. II and also make note of various technical details. We will begin with the calculation of the band structure. From the expansion (14) one is led to the secular equation

$$\sum_{\mathbf{G}'} a_{\mathbf{G}'}(\mathbf{k})(\langle\mathbf{k}+\mathbf{G}\,|\,H_0\,|\,\mathbf{k}+\mathbf{G}'\rangle-\delta_{\mathbf{G},\mathbf{G}'}\epsilon_F)=0\ , \tag{A1}$$

with the matrix elements

$$\langle\mathbf{k}'\,|\,H_0\,|\,\mathbf{k}\rangle=\frac{\hbar^2k^2}{2m}\delta_{\mathbf{k},\mathbf{k}'}+w(\mathbf{k}',\mathbf{k})S(\mathbf{G})D(\mathbf{G})\delta_{\mathbf{k}'-\mathbf{k},\mathbf{G}}\ . \tag{A2}$$

Here $w(\mathbf{k}',\mathbf{k})$ is the pseudopotential form factor of a single ion, $S(\mathbf{G})$ is the structure factor of a unit cell, and $D(\mathbf{G})$ is a Debye-Waller factor [see (15)]. Our w's are nonlocal and derive from fits to low-temperature de Haas–van Alphen data.[46,47] Since for the evaluation of (10) we also need $w(\mathbf{k}',\mathbf{k})$ for general $\mathbf{k}',\mathbf{k}$, we use an interpolation procedure to move away from the points $\mathbf{k}'-\mathbf{k}=\mathbf{G}$ and to match on to the form factors suggested by Shaw[48] or by Appapillai and Williams.[49] These are denoted, respectively, by the initials SOMP (Shaw optimized model potential) and AWSF (Appapillai, Williams, Stark, and Falicov). Up to this point we have followed earlier work;[5–8] differences arise when we try to account for the elevated temperature. Since w represents a screened interaction, we imagine it to have the form $w\sim w^{(b)}/\epsilon$, where $w^{(b)}$ is the "bare" interaction which we assume is independent of the temperature, T. The dielectric constant ϵ is presumed to be the Lindhard function at the appropriate free-electron density. Finally, accounting for the direct scaling of w with atomic density leads to

$$w(\mathbf{k}',\mathbf{k};T)=w(\mathbf{k}',\mathbf{k};T=0)\left[\frac{\Omega_0(0)}{\Omega_0(T)}\frac{\epsilon_L(\mathbf{q},k_F^0(0))}{\epsilon_L(\mathbf{q},k_F^0(T))}\right], \tag{A3}$$

as the way we approximate w at high temperatures. In (A3), Ω_0 is the volume/atom, ϵ_L is the Lindhard function, $\mathbf{q}=\mathbf{k}'-\mathbf{k}$ and k_F^0 is the free-electron wave vector. Typical plots of w's are shown in Fig. 1.

We choose the origin to lie on the midpoint of the line connecting the two atoms in the conventional unit cell.[50] Then

$$S(\mathbf{G})=\cos(\mathbf{G}\cdot\mathbf{d}/2)\ , \tag{A4}$$

where $\mathbf{d}$ is the vector connecting the pair of atoms; it is also a jump vector for the type-A jumps. Only this choice of origin insures that all S's are real, which in turn implies that the a's in (A1) may be taken as real. While this

doesn't matter for the calculation of $\epsilon_{\mathbf{k}}$ and $\mathbf{v}_{\mathbf{k}}$, it will prove useful in (A11) below.

The Fermi surface is described in the extended-zone scheme by the length of k_F versus the spherical polar angles θ and ϕ with $\theta=0$ the c axis and $\phi=0$ connecting nearest neighbors in the basal plane. By symmetry one only needs the solution for $0\le\cos\theta\le 1$ and $0\le\phi\le\pi/6$, although to produce the correct a's for other sectors of the Fermi surface requires careful attention to the allowed symmetry operations of the hcp system.[25] The value of the Fermi energy is adjusted until the k-space volume enclosed by the Fermi surface (or first Brillouin-zone boundary if there is no solution at ϵ_F for a range of θ,ϕ) equals $4\pi^3 n(T)$. Once the Fermi surface is determined, the $\mathbf{v}_{\mathbf{k}}$ are found by numerical differentiation, with no allowance for a possible energy dependence of the pseudopotential.[5]

Next consider the calculation of the X^α. From (11)

$$X^\alpha=\frac{2m}{n\Omega}\sum_{\mathbf{k}}\delta(\epsilon_{\mathbf{k}}-\epsilon_F)(\mathbf{v}_{\mathbf{k}}\cdot\hat{\mathbf{x}}^\alpha)^2$$
$$=\frac{m}{4\pi^3 n\hbar}\oint_{\mathrm{FS}}\frac{dS}{v_{\mathbf{k}}}(\mathbf{v}_{\mathbf{k}}\cdot\hat{\mathbf{x}}^\alpha)^2\,, \tag{A5}$$

where $\hat{\mathbf{x}}^\alpha$ is a unit vector along $\theta=0$ for $\alpha=\|$ or $\theta=\pi/2$ for $\alpha=\perp$ and $v_{\mathbf{k}}=|\mathbf{v}_{\mathbf{k}}|$. The integral over the Fermi surface (FS) is performed by the same Monte Carlo methods described in earlier work.[5]

Finally we examine the $A^{\gamma,\alpha}$ defined in (16)

$$A^{\gamma,\alpha}=\frac{4\pi m}{ne^2}\sum_{\mathbf{k}}\delta(\epsilon_{\mathbf{k}}-\epsilon_F)\sum_{\mathbf{k}'}\delta(\epsilon_{\mathbf{k}'}-\epsilon_F)\int\frac{dR'}{R^\gamma}\mathrm{Im}(\langle\phi_{\mathbf{k}}|U|\phi_{\mathbf{k}'}\rangle\langle\phi_{\mathbf{k}'}|\mathbf{F}\cdot\hat{\mathbf{x}}^\gamma|\phi_{\mathbf{k}}\rangle)(\mathbf{v}_{\mathbf{k}}\cdot\hat{\mathbf{x}}^\alpha)/\hat{\mathbf{x}}^\gamma\cdot\hat{\mathbf{x}}^\alpha\,, \tag{A6}$$

where $\hat{\mathbf{x}}^\gamma$ is a unit vector along the jump direction. If the Bloch pseudo-wave-functions are replaced with plane waves, then one can prove that the $A^{\gamma,\perp}$ are independent of the direction of $\hat{\mathbf{x}}^\perp$ in the basal plane.[25] We checked that within our numerical accuracy this independence also holds when the Bloch states are written as the sum of two plane waves. The $A^{\gamma,\alpha}$ do depend in general on α (see Table III), which implies that the driving force is not parallel to $\mathbf{E}^\alpha$ for jumps between adjacent planes.

With the definition

$$\mathbf{B}(\mathbf{k},\mathbf{k}')=\left[\frac{\Omega}{\Omega_0}\right]^2\int\frac{dR'}{R^\gamma}\mathrm{Im}(\langle\phi_{\mathbf{k}}|U|\phi_{\mathbf{k}'}\rangle\langle\phi_{\mathbf{k}'}|\mathbf{F}|\phi_{\mathbf{k}}\rangle)\,, \tag{A7}$$

we can rewrite (A6) as

$$A^{\gamma,\alpha}=\frac{mZ_d^2}{16\pi^5 n^3 e^2\hbar^2}\oint_{\mathrm{FS}}\frac{dS}{v_{\mathbf{k}}}\oint_{\mathrm{FS}}\frac{dS'}{v_{\mathbf{k}'}}(\mathbf{v}_{\mathbf{k}}\cdot\hat{\mathbf{x}}^\alpha)[\mathbf{B}(\mathbf{k},\mathbf{k}')\cdot\hat{\mathbf{x}}^\gamma]/\hat{\mathbf{x}}^\alpha\cdot\hat{\mathbf{x}}^\gamma\,. \tag{A8}$$

For the calculations of this paper we ignore lattice-distortion effects and write

$$\frac{\Omega}{\Omega_0}\langle\mathbf{k}'|U(\mathbf{R}')|\mathbf{k}\rangle=w(\mathbf{k}',\mathbf{k})[e^{-i\mathbf{q}\cdot\mathbf{R}'}-e^{-i\mathbf{q}\cdot\mathbf{R}_1}D(\mathbf{q})-e^{-i\mathbf{q}\cdot\mathbf{R}_2}D(\mathbf{q})]\,, \tag{A9}$$

where $\mathbf{R}_1$ and $\mathbf{R}_2$ denote the vacancy positions at the ends of the jump path and $\mathbf{q}=\mathbf{k}'-\mathbf{k}$. As discussed in Sec. II, a DWF does not multiply the term associated with the moving atom. Using

$$\mathbf{F}(\mathbf{R}')=-\partial U/\partial\mathbf{R}'\,, \tag{A10}$$

we can easily find matrix elements of F, too. Then with the expansion (14) we obtain

$$\mathbf{B}(\mathbf{k}',\mathbf{k})=\sum_{\substack{\mathbf{G},\mathbf{G}'\\ \mathbf{H},\mathbf{H}'}}(\mathbf{k}+\mathbf{H}-\mathbf{k}'-\mathbf{H}')a_{\mathbf{G}}(\mathbf{k})a_{\mathbf{G}'}(\mathbf{k}')a_{\mathbf{H}'}(\mathbf{k}')a_{\mathbf{H}}(\mathbf{k})\bar{S}w(\mathbf{k}+\mathbf{G},\mathbf{k}+\mathbf{G}')w(\mathbf{k}'+\mathbf{H}',\mathbf{k}+\mathbf{H})\,, \tag{A11}$$

where the sums are over reciprocal-lattice vectors. The quantity $\bar{S}$, which we call the averaged structure factor, may be written as

$$\bar{S}=\cos(\mathbf{M}\cdot\mathbf{R}_1)\left[\frac{\sin(\mathbf{M}\cdot\mathbf{R}^\gamma)}{\mathbf{M}\cdot\mathbf{R}^\gamma}-D(\mathbf{k}+\mathbf{G}-\mathbf{k}'-\mathbf{G}')\left[\frac{\sin(\mathbf{Q}\cdot\mathbf{R}^\gamma)-\sin(\mathbf{M}\cdot\mathbf{R}^\gamma)+\sin[(\mathbf{Q}+\mathbf{M})\cdot\mathbf{R}^\gamma]}{\mathbf{Q}\cdot\mathbf{R}^\gamma}\right]\right]$$
$$-\sin(\mathbf{M}\cdot\mathbf{R}_1)\left[\frac{1-\cos(\mathbf{M}\cdot\mathbf{R}^\gamma)}{\mathbf{M}\cdot\mathbf{R}^\gamma}+D(\mathbf{k}+\mathbf{G}-\mathbf{k}'-\mathbf{G}')\left[\frac{1-\cos(\mathbf{q}\cdot\mathbf{R}^\gamma)-\cos(\mathbf{M}\cdot\mathbf{R}^\gamma)+\cos[\mathbf{Q}+\mathbf{M})\cdot\mathbf{R}^\gamma]}{\mathbf{Q}\cdot\mathbf{R}^\gamma}\right]\right]\,, \tag{A12}$$

where

$$\mathbf{Q}=\mathbf{k}'+\mathbf{H}'-\mathbf{k}-\mathbf{H}\,, \tag{A13}$$
$$\mathbf{M}=\mathbf{G}'-\mathbf{G}-(\mathbf{H}'-\mathbf{H})\,, \tag{A14}$$
$$\mathbf{R}^\gamma=\mathbf{R}_2-\mathbf{R}_1=\hat{\mathbf{x}}^\gamma R^\gamma\,. \tag{A15}$$

An important point in obtaining (A11) is the fact that for our choice of origin the a's are real. In contrast, GH choose the origin at a lattice site, but then ignore the fact that their a's are in general complex. The numerical consequences of this mistake may not be large since to the

extent that the Bloch pseudo-wave-function is well approximated by a single plane wave (as we assume in cases 1–4 of Table III) then $a_0(\mathbf{k})=1$ is real and all other a's vanish. In this single-plane-wave limit (A11) reduces to

$$\mathbf{B}(\mathbf{k}',\mathbf{k})\approx -\mathbf{q}w(\mathbf{k}',\mathbf{k})w(\mathbf{k},\mathbf{k}')\left[1-2D(\mathbf{q})\frac{\sin(\mathbf{q}\cdot\mathbf{R}^{\gamma})}{\mathbf{q}\cdot\mathbf{R}^{\gamma}}\right], \tag{A16}$$

where $\mathbf{q}=\mathbf{k}'-\mathbf{k}$.

The pair of Fermi-surface integrals in (A8) are done by the Monte Carlo methods developed before.[5] A useful check on these is possible in the free-electron limit (case 1) in which the two integrals can be reduced analytically to a single integral over the wave-vector transfer $0\le q\le 2k_F^0$.[51] The fourfold sum in (A11) consumes a lot of time when several plane waves are allowed in $|\phi_{\mathbf{k}}\rangle$. The cgs units of A^{γ} are seconds, which we converted to $\mu\Omega$ cm in Table III.[52]

For all the calculations reported there, the R' integral in (A6) runs along the straight line $\hat{\mathbf{x}}^{\gamma}$. One can prove that in the first four cases the answer must be independent of the path followed; i.e., $\nabla\times\mathbf{F}_w^D=0$.[25] When more than one term is kept in the plane-wave expansion of the Bloch pseudo-wave-function in the matrix elements, this result no longer holds. We found for several case-5 calculations a slight path dependence of the work done by $\mathbf{F}_w^D$. However, the deviations of the diffusion path from a straight line reasonably possible in a close packed system do not allow for much variation. The resulting uncertainty in our answers is much less than that due to Δ in (23).

[1]J. L. Routbort, Phys. Rev. **176**, 796 (1968).
[2]H. B. Huntington, W. B. Alexander, M. D. Feit, and J. L. Routbort, in *Proceedings of the Conference on Atomic Transport in Solids and Liquids, Marstand, 1970,* edited by A. Lodding and T. Lagerwall (Verlag, Tubingen, 1971), p. 91.
[3]W. B. Alexander, Z. Naturforsch. Teil A **26**, 18 (1971); in *Proceedings of the Conference on Atomic Transport in Solids and Liquids, Marstand, 1970,* Ref. 2, p. 97.
[4]J. Wohlgemuth, J. Phys. Chem. Solids **36**, 1025 (1975).
[5]P. G. Tomlinson and J. C. Swihart, Phys. Rev. B **19**, 1867 (1979).
[6]P. G. Tomlinson, Phys. Rev. B **19**, 1893 (1979).
[7]M. P. Pepchinski and J. C. Swihart (unpublished).
[8]W. Chen, J. C. Swihart, and W. E. Lawrence, Bull. Am. Phys. Soc. **30**, 429 (1985).
[9]W. L. Schaich, Phys. Rev. B **13**, 3350 (1976).
[10]T. C. Genoni and H. B. Huntington, Phys. Rev. B **16**, 1344 (1977).
[11]W. C. Chan and H. B. Huntington, Phys. Rev. B **12**, 5441 (1975).
[12]H. B. Huntington in *Diffusion in Solids, Recent Developments,* edited by A. S. Nowick and J. J. Burton (Academic, New York, 1975), p. 303.
[13]R. S. Sorbello, Comments Solid State Phys. **6**, 117 (1975).
[14]R. S. Sorbello, in *Electro- and Thermo-transport in Metals and Alloys,* edited by R. E. Hummel and H. B. Huntington (Metallurgical Society of AIME, New York, 1977), p. 2.
[15]W. L. Schaich, in *Liquid Metals, 1976,* edited by R. Evans and D. Greenwood (IOP, Bristol, 1977), p. 638.
[16]P. Kumar and R. S. Sorbello, Thin Solid Films **25**, 25 (1975).
[17]R. P. Gupta, Phys. Rev. B **25**, 5188 (1982).
[18]R. P. Gupta, Y. Serruys, G. Brebec, and Y. Adda, Phys. Rev. B **27**, 672 (1983).
[19]R. S. Sorbello, A. Lodder, and S. J. Hoving, Phys. Rev. B **25**, 6178 (1982).
[20]A. Lodder, J. Phys. F **14**, 2943 (1984).
[21]A. Lodder and M.G.E. Brand, J. Phys. F **14**, 2955 (1984).
[22]W. L. Schaich, Phys. Rev. B **13**, 3360 (1976).
[23]L. J. Sham, Phys. Rev. B **12**, 3142 (1975).
[24]L. J. Sham, Proc. Phys. Soc. London **98**, 895 (1961).
[25]L. Lou (unpublished).
[26]L. A. Girifalco, *Atomic Migration in Crystals* (Blaisdell, New York, 1964).
[27]Since B jumps are orthogonal to the c axis, no $Z_w^{B,\parallel}$ is necessary.
[28]P. B. Allen and V. Heine, J. Phys. C **9**, 2305 (1976).
[29]E. F. Skelton and J. L. Katz, Phys. Rev. **171**, 801 (1968).
[30]Chosen along with T to agree with GH; see T. C. Genoni, J. Phys. F **7**, 1867 (1977).
[31]W. B. Pearson, *A Handbook of Lattice Spacings and Structure of Metals* (Pergamon, London, 1964).
[32]Y. Watanabe, H. Iwaski, and S. Ogawa, Jpn. J. Appl. Phys. **10**, 786 (1971).
[33]D. Sledziewska-Blocka and A. Rajca, J. Phys. Chem. Solids **35**, 181 (1974).
[34]J. M. Ziman, Philos Mag. **6**, 1013 (1961).
[35]T. E. Faber, *Introduction to the Theory of Liquid Metals* (Cambridge University Press, London, 1972).
[36]N. W. Ashcroft and J. Lekner, Phys. Rev. **145**, 83 (1966).
[37]C. J. Smithells, *Metals Reference Book* (Butterworths, London, 1967), Vol. 3.
[38]P. G. Shewmon, *Diffusion in Solids* (McGraw-Hill, New York, 1963).
[39]J. G. Mullen, Phys. Rev. **124**, 1723 (1961).
[40]N. L. Peterson and S. J. Rothman, Phys. Rev. **163**, 645 (1967).
[41]C. W. Mao, Phys. Rev. B **5**, 4693 (1972).
[42]P. G. Shewmon, J. Metals N.Y. **8**, 918 (1956).
[43]J. Bass in *Metals: Electronic Transport Phenomena,* Vol. 15A of *Landolt-Bornstein, Numerical Data and Functional Relationships in Science and Technology,* edited by K.-H. Hellwege and J. L. Olsen (Springer, New York, 1982), p. 1.
[44]G. Beni and P. M. Platzman, Phys. Rev. B **14**, 1514 (1976).
[45]E. Sevillano, H. Meuth, and J. J. Rehr, Phys. Rev. B **20**, 4908 (1979).
[46]R. W. Stark and L. M. Falicov, Phys. Rev. Lett. **19**, 795 (1967).
[47]J. C. Kimball, R. W. Stark, and F. M. Mueller, Phys. Rev. **162**, 600 (1967).
[48]R. W. Shaw, Jr., J. Phys. C **2**, 2335 (1969); Phys. Rev. **174**, 769 (1968).
[49]M. Appapillai and A. R. Williams, J. Phys. F **3**, 759 (1973).
[50]C. Kittel, *Introduction to Solid State Physics* (Wiley, New York, 1976).
[51]R. S. Sorbello, J. Phys. Chem. Solids **34**, 937 (1973).
[52]J. D. Jackson, *Electrodynamics* (Wiley, New York, 1975).